Huygens-Fresnel Acoustic Interference and the Development of Robust Time-Averaged Patterns from Traveling Surface Acoustic Waves

Citsabehsan Devendran,[1] David J. Collins,[2] Ye Ai,[2] and Adrian Neild[1,*]
[1]Laboratory for Micro Systems, Department of Mechanical and Aerospace Engineering, Monash University, Melbourne 3800, Victoria, Australia
[2]Pillar of Engineering Product Development, Singapore University of Technology and Design, Singapore 487372, Singapore
(Received 10 October 2016; published 12 April 2017)

Periodic pattern generation using time-averaged acoustic forces conventionally requires the intersection of counterpropagating wave fields, where suspended micro-objects in a microfluidic system collect along force potential minimizing nodal or antinodal lines. Whereas this effect typically requires either multiple transducer elements or whole channel resonance, we report the generation of scalable periodic patterning positions without either of these conditions. A single propagating surface acoustic wave interacts with the proximal channel wall to produce a knife-edge effect according to the Huygens-Fresnel principle, where these cylindrically propagating waves interfere with classical wave fronts emanating from the substrate. We simulate these conditions and describe a model that accurately predicts the lateral spacing of these positions in a robust and novel approach to acoustic patterning.

DOI: 10.1103/PhysRevLett.118.154501

Ultrasonic acoustic fields are applicable to a number of industrial and clinical processes, where the resultant acoustic forces permit the noncontact manipulation of macroscale objects, microparticles, and biological cells. Notable and diverse examples of acoustic manipulation include an acoustic tractor beam [1,2], acoustic levitation systems [3–5], particle patterning and positioning [6–8], and continuous sorting according to size and mechanical properties [9,10]. Acoustic fields are especially interesting for microscale biological processing, where acoustic wavelengths can be generated on the scale of tens of microns or smaller [11] for the long-term patterning and culture of cells [12,13]. There are a number of acoustic actuation technologies at the microscale, using bulk acoustic waves (BAW) to excite channel resonances [14–17], coupled substrate vibrations from surface acoustic waves (SAW) [18,19], and thin-membrane oscillations [20,21] to develop spatially periodic patterning. The patterning mechanism in each case, however, remains effectively the same, where the intersection of a propagating and counterpropagating or reflected acoustic waves results in time-averaged minimum pressure nodes to which suspended particles typically migrate, spaced $1/2$ of an acoustic wavelength (λ_{ac}) apart.

While traveling waves can also be utilized for microscale manipulation and continuous sorting [22,23], the time-averaged force arising from scattering is continuous in the propagation direction, albeit exponentially decaying, rather than periodic. Particle patterning can, however, be achieved using holographic methods at the intersection of phase shifted wave fronts [24,25] at either side of a surface acoustic wave generated beam [26] or with intersecting traveling waves. In the latter case, the minimum pressure location(s) can be predicted from the rectilinear acoustic propagation model [27], which is widely used when considering SAW systems.

However, there have been a limited number of observations of particle patterning with the imposition of traveling waves that are not accounted for by rectilinear traveling wave fronts [7,28]. An alternative, less simplified, model for describing the propagation of acoustic energy is that according to the Huygens-Fresnel principle, where every point on an advancing wave front can be represented as a spherical wave source [29]. Considered in a three-dimensional domain symmetric about the plane of interest (i.e., the x-z plane projected in the y direction), this takes the form of a cylindrical wave source. While this model is necessary to describe interference patterns in the classical double-slit experiment, it has not been a common feature in describing microscale acoustofluidic phenomenon, where the small fluid acoustic attenuation values at even MHz frequencies generally lead to reflections and the resulting predominance of acoustic standing waves. A substrate-bound wave such as a Rayleigh-mode SAW, however, offers shorter acoustic attenuation lengths than other wave modes [30] that can also be orders of magnitude smaller than the fluid one, $\approx 10\ \lambda_{SAW}$ for common substrate materials [22,31], minimizing reflections and allowing traveling wave dominant force fields.

In this work we describe the development of robust time-averaged spatial periodicity in acoustic force potential gradients from the imposition of a traveling wave incident with a water-filled microchannel [Fig. 1(a)]. We present experimental results which demonstrate microfluidic particle patterning that can extend 10's of SAW wavelengths along the substrate. In a system where this effect is predominant, this represents a novel mechanism for microfluidic patterning that permits utility not available with

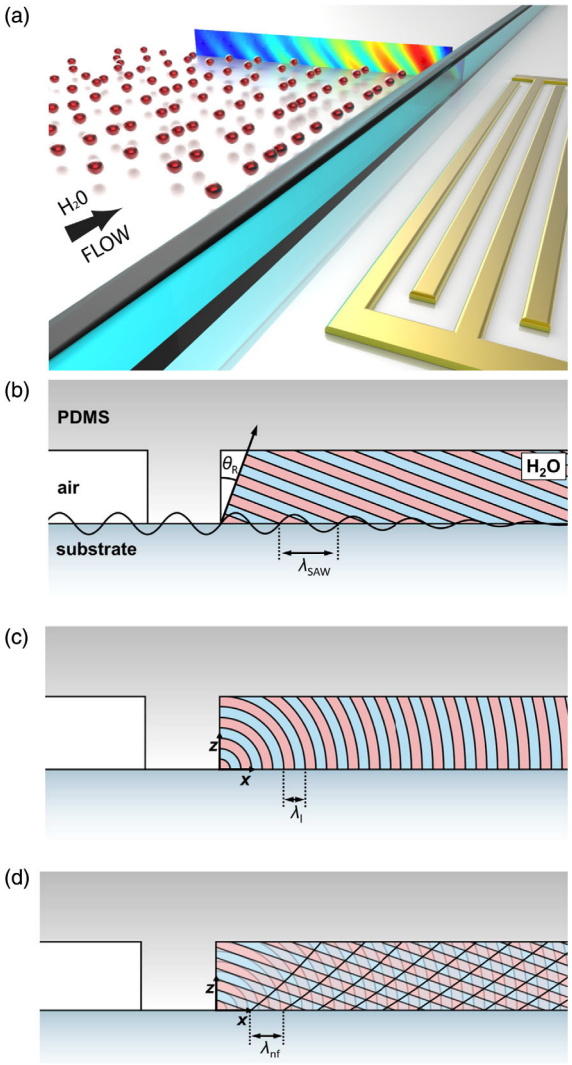

FIG. 1. Principle of acoustic self-interaction and resulting time-averaged near-field patterning. (a) Three-dimensional drawing of a typical TSAW driven acoustofluidic systems with PDMS confined microchannels exhibiting particle patterning in the near field. (b) The classical model predicts the emergence of unified wave fronts propagating from substrate vibrations with wavelength λ_{SAW} into the liquid domain at the Rayleigh angle, θ_R. (c) According to the Huygens-Fresnel principle, each point along a wave front (both on the substrate and in the fluid) generates a cylindrically propagating wave with λ_l, here shown from the PDMS-water-substrate contact points, which when superimposed result in the unified wave fronts in (b). (d) The asymmetric, one-sided source of these cylindrical waves (the knife-edge effect) and their interactions results in time-averaged positions of maximum and minimum displacement velocities in the fluid, with periodic spacing λ_{nf} as $z \to 0$.

standing waves; the patterning extent scales with applied power, permitting particle alignment in a modifiable subset of a microfluidic channel.

This periodicity can be explained via numerical and analytical models which combine the interaction of a planar wave front emanating from the oscillating substrate propagating through the fluid at the Rayleigh angle, $\theta_R = \sin^{-1}(c_1/c_s)$ as shown in Fig. 1(b), where c_l and c_s are the sound speeds in the liquid and solid phases, respectively, with the cylindrically propagating wave front emanating from the three-material contact line where the SAW enters the channel. This cylindrical wave front is a manifestation of the Huygens-Fresnel principle, which states that each point across the transducer's face emits a wavelet, and where a transducer edge serves as an effective point source of these wavelets [32,33]. A common method of calculating the resulting interference pattern is via the convolution of the impulse response and excitation wave form [34]. The former is a geometrically calculated measure at each location related to the number of these wavelets which will arrive over time. An alternative approach examines the time differential of the impulse response. Here the impulse response changes most significantly when the first wavelet arrives, and when the number of wavelets first starts to decay. This is akin to the arrival of a plane wave from the face of the transducer followed by an edge wave from the periphery [35]. In our case, the plane wave emanates from the substrate at θ_R, and the edge wave from the three material contact point; having reduced the system to these two wave fronts, we analytically calculate the regions of pressure minima and maxima.

The SAW based acoustofluidic device consists of a 500 μm thick 128° Y-cut X-propagating lithium niobate ($LiNbO_3$; LN) piezoelectric crystal patterned with interdigital transducers (IDTs) and bonded to a PDMS microchannel (Fig. 1). These transducers are 7 mm wide, and positioned approximately 2 mm from the channel edge, a combination that minimizes the effect of diffraction induced amplitude distortions across the beam width [36]. The IDTs are excited with a harmonic signal at the resonant frequency $f = c_s/\lambda_{\mathrm{SAW}}$, resulting in a TSAW along the substrate [37]. To demonstrate the applicability of the effect for systems incorporating throughput, a particle solution flows past the transducer with a continuous velocity and is imaged in the middle of the SAW aperture. To capture the dynamics of our system, we propose a modeled domain consisting of the two-dimensional fluid coupled to a piezoelectric, LN substrate. The PDMS walls are replaced using a radiation boundary condition that ensures minimal reflections at the upper and distal channel wall boundaries. Radiation boundary conditions are implemented with the sole purpose of clearly demonstrating the inherent Huygens-Fresnel interference pattern. Experimentally, we expect additional effects arising from wave reflections due to the acoustic impedance mismatch at the PDMS-fluid interface, discussed in more detail within the experimental section. The computational domain consists of a rectangular liquid-filled chamber with a corresponding height h, width W, and a varied liquid speed of sound, c_1 at a constant substrate Rayleigh-mode sound speed, $c_s = 3994$ ms^{-1}.

An analytical description of the periodic field along the propagation direction can be found directly from geometric considerations, namely, from the intersection

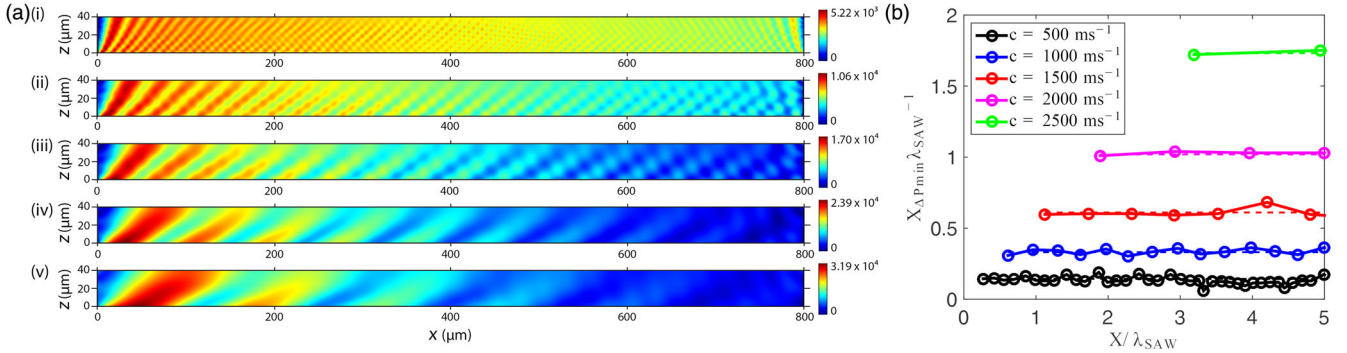

FIG. 2. (a) Surface plots for a $W = 800$ μm (i.e., 10 λ_{SAW}) and $h = 40$ μm (i.e., 0.5 λ_{SAW}) system of the resultant time-averaged modulus of the first-order pressure fields, $\langle|P_1|\rangle$ for fluid mediums corresponding to a speed of sound, c_1 of (i) 500,(ii) 1000, (iii) 1500, (iv) 2000, and (v) 2500 ms^{-1}. (b) Plot depicting the spacing between the local time-averaged pressure minima, ΔP_{min} locations normalized by the SAW wavelength λ_{SAW}, at $z = 5$ μm against the corresponding normalized pressure minima location in the x direction (dashed lines are average values).

of the cylindrical wave fronts propagating through the fluid with those emanating from the oscillating substrate; these cylindrical waves can be approximated as horizontal wave fronts, appropriate for $z \to 0$ and for increasing x values (see Supplemental Material [38], Note 1). These traveling wave fronts create static interference patterns despite their continuous propagation through the fluid (see Supplemental Material [38], Video 1) and result in time-averaged pressure maxima locations. Along a given width in the x direction, this yields a near-field patterning distance in the plane of the substrate-fluid interface, given by

$$\lambda_{\mathrm{nf}} = \lambda_{\mathrm{l}} \cot\left[\frac{1}{2}\left(\frac{\pi}{2}\right) - \theta_R\right] \sec(\theta_R), \tag{1}$$

where θ_R is the Rayleigh angle and λ_l is the wavelength in the liquid, related to that of the SAW substrate by $\lambda_{\mathrm{l}} = (c_{\mathrm{l}}/c_{\mathrm{s}})\lambda_{\mathrm{SAW}}$. Substituting $\theta_R = \sin^{-1}(c_{\mathrm{l}}/c_{\mathrm{s}})$, we can recast Eq. (1) in terms of the ratio of the liquid and substrate sound speed

$$\lambda_{\mathrm{nf}} = \lambda_l\left(1 - \frac{c_{\mathrm{l}}}{c_{\mathrm{s}}}\right)^{-1}, \tag{2}$$

valid for wave front propagation from a substrate-bound Rayleigh wave at θ_R, where $c_l < c_s$; when $c_l > c_s$ only an evanescent wave at the interface develops without penetration into the fluid bulk [21], precluding the generation of wave fronts that intersect with the cylindrically propagating edge ones. In the system considered here, the electrodes are designed to efficiently excite surface acoustic waves, for which $c_l < c_s$. The angle at which the maximum (and minimum) fluid displacement locations project into the fluid from the substrate-fluid interface is given by

$$\theta_{\mathrm{nf}} = \frac{1}{2}\cos^{-1}\left(\frac{c_l}{c_s}\right). \tag{3}$$

While the analytical model approach sets up this intersection condition explicitly, it is an emergent feature of the simulated one. As illustrated in Fig. 2(a) (i–v), we observe a time-averaged absolute pressure, $\langle|P_1|\rangle$ field with a spatial pressure distribution consisting of local minima and maxima locations arising from the edge effect at the leftmost channel extent and the TSAW coupled along the substrate-fluid medium interface. The observed pressure distribution is established in accordance with the Huygens-Fresnel principle, analogous to the case of a multitransducer ultrasonic beam [39], where diffraction effects generate multilobed near-field amplitude patterns. This effect has been briefly shown in recent simulation results [7,40]; here we attempt to note the key features and quantify this effect in light of the physical parameters that give rise to it. Noticeably, the amplitudes of the high pressure regions (in red) decrease as x increases due to the inherent decay of leaky SAW as it couples energy into the fluid [26,40]. Furthermore, as the speed of sound of the fluid medium is increased from 500 to 2500 ms^{-1} [as illustrated in Fig. 2(a)], the spacing between the pressure minima locations, $x_{\Delta\mathrm{Pmin}}$ (i.e., particle collection locations) similarly increases. These spacings are normalized by the

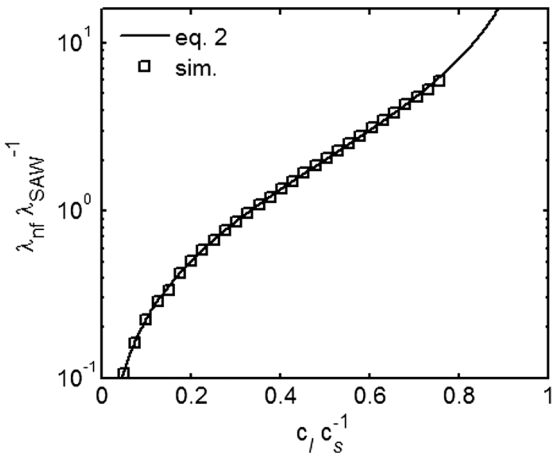

FIG. 3. Comparison of the analytical model [Eq. (2)] with simulated horizontal periodicity. We compute the near-field patterning spacing λ_{nf} from $c_{\mathrm{l}}c_{\mathrm{s}}^{-1} = 0$ to $c_{\mathrm{l}}c_{\mathrm{s}}^{-1} = 1$, with increasing λ_{nf} as $c_{\mathrm{l}} \to c_{\mathrm{s}}$. These calculated values are matched by those computed from the simulations as in Fig. 2.

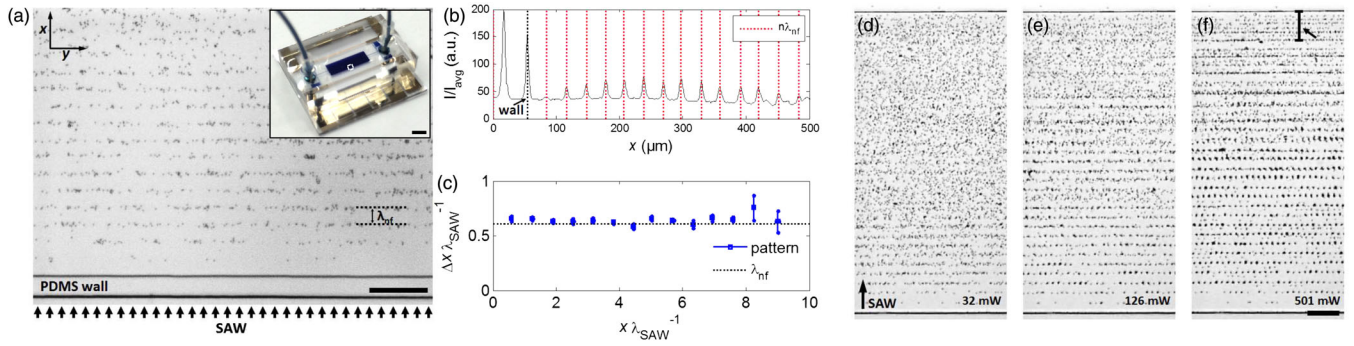

FIG. 4. Particle patterning due to near-field interactions. (a) A 48 μm, 81 MHz traveling SAW at 64 mW generates a near-field period force field whose acoustic force magnitude decays with increasing distance due to attenuation at the substrate-water interface. This force field is used to pattern suspended 2 μm polystyrene particles. Inset shows the macroscopic device (scale bar 200 μm). These patterning positions are measured across 143 separate frames (at 20 fps), where (b) shows a representative measurement, yielding (c) average particle positions corresponding to the predicted patterning spacing. (d)–(f) The penetration of this near-field effect scales with increasing applied power, though the effects of channel reflections, and thus the influence of standing waves, becomes apparent when the SAW amplitude is of sufficient magnitude to realize these effects at the distal channel wall. Scale bars are 100 μm.

SAW wavelength, $x_{\Delta\mathrm{Pmin}}\lambda_{\mathrm{SAW}}{}^{-1}$ along the x propagating direction at a height near the substrate, $z = 5$ μm and are plotted in Fig. 2(b). These are in good agreement with the analytical predictions outlined in Eq. (2) and Fig. 3, and represent a stark contrast to a standing wave system in which the pressure minima locations at all wave speeds would lie along $0.5\ x_{\Delta\mathrm{Pmin}}\lambda_{\mathrm{SAW}}{}^{-1}$. Notably, the amplitude decay of the pressure fields are more significant in mediums corresponding to a higher c_l. As $c_l \to c_s$ the coupling of energy into the fluid medium increases [31,41], resulting in increased SAW attenuation.

We confirm these predictions in an experimental setup that is a good match for the aspect ratio in the simulated system, where particles are vertically confined in a $h \approx 20$ μm high channel to limit the number of stable vertical positions particles are patterned and minimize streaming [40]. The effects of acoustic streaming are further minimized by reducing the substrate displacement gradients that would give rise to streaming, namely, by using transducer apertures that are wider than the channel length (e.g., a 9 mm wide, 48 μm IDT in a 6 mm long channel). The small reflection coefficient at the water-PDMS interface ($\approx 4\%$) results in a vertical time-averaged field component that is superimposed on the near-field one; a $\lambda_{\mathrm{SAW}} = 48$ μm substrate wave results in vertical periodicity on the order of this channel height (Supplemental Material [38], Video 2, 0.3 μl/ min flow rate). Supplemental Material [38], Video 3 (0.5 μl/ min flow rate) and Fig. S2 (see Supplemental Material [38], Note 2) demonstrates the same near-field patterning effect, however, with a slightly higher channel height with respect to the acoustic wavelength ($\lambda_{\mathrm{SAW}} = 80$ μm, h ≈ 42 μm), permitting multiple distinct heights at which particles are patterned. These multiple heights are present due to the reflection of the incident wave at the PDMS-fluid interface, which gives rise to a vertical periodicity in the resultant pressure field (see Supplemental Material [38], Note 2). Interactions with the opposing channel wall are minimized by maximizing the amount the SAW is attenuated at the point where it partially reflects off it. Here we use a channel much wider than the height dimension. In the case of a 2000 μm width, corresponding to $\approx$3.4 SAW attenuation lengths, the SAW displacement is 4% at the opposing wall, and where only a fraction of that displacement will be reflected back to the proximal wall. Notably, the near-field effect under investigation in this work is capable of exerting appreciable forces on submicron particles; Supplemental Material [38], Video 4 (0.2 μl/ min flow rate, $\lambda_{\mathrm{SAW}} = 71$ μm, $h \approx 25$ μm) shows the long-term convergence of 500 nm particles in the aforementioned patterns despite the increasing influence of streaming on particle trajectories with decreasing particle size [40,42].

This periodic near-field is visualized in Fig. 4(a), which shows patterned 2 μm particles suspended in water with diminishing focusing behavior with increasing distance from the channel wall, reflecting the decreasing acoustic force potential gradient magnitudes with decreasing SAW amplitude. Figures 4(b), 4(c) show the measured particle positions and spacing (image intensity averaged across the width of the frame) as compared to those predicted from Eq. (3), with a measured average spacing of 0.63 ± 0.03 λ_{SAW} as compared to the 0.61 λ_{SAW} spacing predicted from Eq. (2), and distinctly larger than the 0.5 λ_{SAW} spacing in the case of a substrate-bound standing wave [43]. Figures 4(d)–4(f) demonstrate the scalability of this effect; by increasing the applied power, the region in which the acoustic field magnitude is sufficient to focus particles is (linearly) expanded. By using a narrower 1000 μm channel the effect of reflection off the opposing interface is observed: the particle spacing is much closer in the vicinity of the distal channel wall in Fig. 4(f) due to fluid wave fronts reflecting and interacting with incoming ones (standing waves) in the vicinity of the weakly reflective PDMS-water interface, with periodicity corresponding to 0.5 λ_l. This is only noted at the higher applied powers (here at 501 mW) required for particle translation at this location.

In summary, we have described and analyzed a phenomenon where the imposition of a traveling wave can, through acoustic self-interaction, result in the generation of a time-averaged spatially periodic field along the axis of acoustic propagation, as demonstrated here for a microfluidic SAW device. In the construction of a straightforward analytical model with confirming simulation and experimental results, we have demonstrated that this effect can be explained by the combination of the classical wave fronts emanating from a substrate with those arising from the edge effect, where a discontinuity along the oscillating substrate serves as the progenitor of cylindrically propagating waves. This effect is most pronounced in systems that are scaled to take advantage of it, namely, those whose dimensions are on the order or exceed the attenuation lengths of the acoustic field driving the microfluidic phenomena. As acoustofluidic systems increasingly utilize frequencies approaching and exceeding 1 GHz for refined nanoscale manipulation [11,26], this characteristic will be increasingly represented. We envision that this new particle manipulation technique, namely, the generation of spatially limited acoustic patterning locations using traveling waves emanating from a single transducer, will be a viable technique for microfluidic manipulation along with forces that result from conventionally applied standing waves, traveling waves, and acoustic streaming.

We gratefully acknowledge support received from the Australian Research Council, Grant No. DP160101263 awarded to A. N. This work was performed in part at the Melbourne Centre for Nanofabrication (MCN) in the Victorian Node of the Australian National Fabrication Facility (ANFF). This research was undertaken with the assistance of resources from the National Computational Infrastructure (NCI), which is supported by the Australian Government. We gratefully acknowledge support received from Singapore Ministry of Education Academic Research Fund Tier 2 (T2MOE1603) awarded to Y. A.

C. D. and D. J. C. contributed equally to this work.

*adrian.neild@monash.edu

[1] C. E. M. Démoré, P. M. Dahl, Z. Yang, P. Glynne-Jones, A. Melzer, S. Cochran, M. P. MacDonald, and G. C. Spalding, Phys. Rev. Lett. **112**, 174302 (2014).
[2] A. Marzo, S. A. Seah, B. W. Drinkwater, D. R. Sahoo, B. Long, and S. Subramanian, Nat. Commun. **6** , 8661 (2015).
[3] M. A. B. Andrade, N. Pérez, and J. C. Adamowski, Appl. Phys. Lett. **106**, 014101 (2015).
[4] S. Tsujino and T. Tomizaki, Sci. Rep. **6**, 25558 (2016).
[5] C. Devendran, D. R. Billson, D. A. Hutchins, and A. Neild, Sensors and Actuators B: Chemical **224**, 529 (2016).
[6] A. Lamprecht, S. Lakamper, T. Baasch, I. A. T. Schaap, and J. Dual, Lab Chip **16**, 2682 (2016).
[7] D. J. Collins, C. Devendran, Z. Ma, J. W. Ng, A. Neild, and Y. Ai, Sci. Adv. **2**, e1600089 (2016).
[8] Q. Zhou, V. Sariola, K. Latifi, and V. Liimatainen, Nat. Commun. **7**, 12764 (2016).
[9] P. Li, Z. Mao, Z. Peng, L. Zhou, Y. Chen, P.-H. Huang, C. I. Truica, J. J. Drabick, W. S. El-Deiry, M. Dao, S. Suresh, and T. J. Huang, Proc. Natl. Acad. Sci. U.S.A. **112**, 4970 (2015).
[10] P. Augustsson, J. T. Karlsen, H.-W. Su, H. Bruus, and J. Voldman, Nat. Commun. **7**, 11556 (2016).
[11] R. J. Shilton, M. Travagliati, F. Beltram, and M. Cecchini, Adv. Mater. **26**, 4941 (2014).
[12] D. J. Collins, B. Morahan, J. Garcia-Bustos, C. Doerig, M. Plebanski, and A. Neild, Nat. Commun. **6**, 8686 (2015).
[13] K. Chen, M. Wu, F. Guo, P. Li, C. Y. Chan, Z. Mao, S. Li, L. Ren, R. Zhang, and T. J. Huang, Lab Chip **16**, 2636 (2016).
[14] B. W. Drinkwater, Lab Chip **16**, 2360 (2016).
[15] I. Leibacher, P. Reichert, and J. Dual, Lab Chip **15**, 2896 (2015).
[16] M. Antfolk, C. Magnusson, P. Augustsson, H. Lilja, and T. Laurell, Anal. Chem. **87**, 9322 (2015).
[17] C. Devendran, I. Gralinski, and A. Neild, Microfluidics Nanofluidics **17**, 879 (2014).
[18] G. Destgeer and H. J. Sung, Lab Chip **15**, 2722 (2015).
[19] J. Shi, D. Ahmed, X. Mao, S.-C. S. Lin, A. Lawit, and T. J. Huang, Lab Chip **9**, 2890 (2009).
[20] G. Vuillermet, P.-Y. Gires, F. Casset, and C. Poulain, Phys. Rev. Lett. **116**, 184501 (2016).
[21] V. Aubert, R. Wunenburger, T. Valier-Brasier, D. Rabaud, J.-P. Kleman, and C. Poulain, Lab Chip **16**, 2532 (2016).
[22] D. J. Collins, A. Neild, and Y. Ai, Lab Chip **16**, 471 (2016).
[23] G. Destgeer, K. H. Lee, J. H. Jung, A. Alazzam, and H. J. Sung, Lab Chip **13**, 4210 (2013).
[24] K. Melde, A. G. Mark, T. Qiu, and P. Fischer, Nature (London) **537**, 518 (2016).
[25] G. Memoli, M. Caleap, M. Asakawa, D. R. Sahoo, B. W. Drinkwater, and S. Subramanian, Nat. Commun. **8**, 14608 (2017).
[26] D. J. Collins, Z. Ma, and Y. Ai, Anal. Chem. **88**, 5513 (2016).
[27] B.-T. Chu and R. E. Apfel, J. Acoust. Soc. Am. **72**, 1673 (1982).
[28] O. Manor, L. Y. Yeo, and J. R. Friend, J. Fluid Mech. **707**, 482 (2012).
[29] H. G. Kraus, J. Opt. Soc. Am. A **6**, 1196 (1989).
[30] G. Lindner, J. Phys. D **41**, 123002 (2008).
[31] M. B. Dentry, L. Y. Yeo, and J. R. Friend, Phys. Rev. E **89**, 013203 (2014).
[32] A. Hayman and J. Weight, J. Acoust. Soc. Am. **66**, 945 (1979).
[33] J. Weight and A. Hayman, J. Acoust. Soc. Am. **63**, 396 (1978).
[34] A. Neild, D. Hutchins, and D. Billson, Ultrasonics **42**, 859 (2004).
[35] S. M. Kramer, S. L. McBride, H. D. Mair, and D. Hutchins, IEEE Trans. Ultrason. Ferroelectr. Freq. Control **35**, 253 (1987).
[36] A. R. Rezk, O. Manor, J. R. Friend, and L. Y. Yeo, Nat. Commun. **3**, 1167 (2012).
[37] L. Y. Yeo and J. R. Friend, Annu. Rev. Fluid Mech. **46**, 379 (2014).
[38] See Supplemental Material at http://link.aps.org/supplemental/10.1103/PhysRevLett.118.154501 for Supplementary Video 1: Model of the intersection of both cylindrical and conventional SAW wavefronts, resulting in time-averaged max/min displacement locations along the SAW propagation direction. Supplementary Video 2: Experimental video of 2 μm diameter polystyrene particle

patterning in the vicinity of a microchannel wall. $\lambda_{SAW} = 48\ \mu$m, $h = 20\ \mu$m. Supplementary Video 3: Experimental video of 1 μm diameter polystyrene particle patterning in the vicinity of a microchannel wall, with patterning at multiple channel heights. $\lambda_{SAW} = 80\ \mu$m, $h = 42\ \mu$m. Supplementary Video 4: Experimental video of 500 nm diameter polystyrene particle patterning in the vicinity of a microchannel wall, with patterning at multiple channel heights. $\lambda_{SAW} = 72\ \mu$m, $h = 25\ \mu$m. Supplementary Note: (1) Geometric derivation of the analytical model (Eq. (1)). (2) Stable pattern formation in the z-direction as a result of reflections from the channel roof.

[39] S.-C. Wooh and Y. Shi, J. Nondestruct. Eval. **18**, 39 (1999).
[40] C. Devendran, T. Albrecht, J. Brenker, T. Alan, and A. Neild, Lab Chip **16**, 3756 (2016).
[41] M. Gedge and M. Hill, Lab Chip **12**, 2998 (2012).
[42] P. B. Muller, R. Barnkob, M. J. H. Jensen, and H. Bruus, Lab Chip **12**, 4617 (2012).
[43] D. J. Collins, T. Alan, and A. Neild, Lab Chip **14**, 1595 (2014).